



Selective and fast recovery of rare earth elements from industrial wastewater by porous β -cyclodextrin and magnetic β -cyclodextrin polymers

François Nkinahamira^{a, b}, Alaaeddin Alsbaiee^c, Qiaoting Zeng^a, Yan Li^{a, b},
Yiqing Zhang^{a, b}, Meiling Feng^d, Chang-Ping Yu^{a, e}, Qian Sun^{a, *}

^a CAS Key Laboratory of Urban Pollutant Conversion, Institute of Urban Environment, Chinese Academy of Sciences, China

^b University of Chinese Academy of Sciences, China

^c Department of Chemistry and Chemical Biology, Cornell University, Ithaca, NY, 14853, USA

^d State Key Laboratory of Structural Chemistry, Fujian Institute of Research on the Structure of Matter, Chinese Academy of Sciences, China

^e Graduate Institute of Environmental Engineering, National Taiwan University, Taiwan

ARTICLE INFO

Article history:

Received 11 December 2019

Received in revised form

7 April 2020

Accepted 20 April 2020

Available online 20 May 2020

Keywords:

Rare earth elements (REEs)

Magnetic composite

Adsorption

Selectivity

Recovery

ABSTRACT

Recovery of rare earth elements (REEs) from industrial wastewater has drawn great attention due to their potential environmental toxicity, as well as their high demand in modern technologies. In this study, we developed a magnetic composite based on the high surface area porous β -cyclodextrin polymer (**P-CDP**), namely **P-CDP@Fe₃O₄**. Both **P-CDP** and **P-CDP@Fe₃O₄** rapidly sequester REEs such as Nd, Gd, Eu, and Y, reaching equilibrium in less than 10 min and fitting the Langmuir isotherm model with maximum adsorption capacities ranging from 7.76 to 9.59 mg/g at 25 °C when the highest initial concentration was 100 mg/L. Besides, the recovery of these REEs was not affected by competitive alkali, alkaline earth, and transition metal ions in model studies and industrial wastewater as revealed by the recovery efficiencies, which ranged from 62% to 100% indicating an excellent selectivity on both adsorbents. In addition, both adsorbents can be fully regenerated under mildly acidic conditions for at least five consecutive cycles. Moreover, **P-CDP@Fe₃O₄** can be easily isolated by an external magnetic field which simplifies its synthesis and usability. It also overcomes the clogging and high backpressure issues of **P-CDP**, which facilitates its application for REEs recovery as compared with **P-CDP**. These characteristics demonstrate the promise of **P-CDP** and **P-CDP@Fe₃O₄** for the pollution control and recovery of REEs.

© 2020 Elsevier Ltd. All rights reserved.

1. Introduction

Rare-earth elements (REEs) have been progressively used in various industries including automobile, electronics, medicine, cosmetics, and renewable energy technologies (Wang et al., 2017; Zhang et al., 2016). In 2012, the department of energy in the USA issued a report considering REEs as crucial elements in the clean energy economy (U.S. department of energy, 2011). China, as a global leader of the REEs market, accounted for 88% of REEs refined products in 2017 (U.S. Geological Survey, 2019). Besides the economic impact, relatively large quantities of REEs, resulting from their mining and production processes, are wide spread in

wastewater, sludge, surface water, soils, plants, and animals. This has raised concerns about the potential negative health effects and environmental toxicity of REEs (Gwenzi et al., 2018; Nkinahamira et al., 2019), and recently REEs were reported as new emerging pollutants (Herrmann et al., 2016; Pagano et al., 2016). Therefore, an efficient technology for the removal and recovery of REEs is urgently needed.

Solvent extraction, chemical precipitation, electrochemical separation, coagulation, and membrane filtration are the most commonly used methods for separation and enrichment of REEs (Gok, 2014). However, these methods are not economical and the separated REEs are not sufficiently recovered after treatment. Additionally, some of these methods generate additional waste such as sludge and toxic solvents (Jha et al., 2016). On the other hand, the adsorption method is simple, relatively more economical and especially effective to remove REEs at environmental

* Corresponding author.

E-mail address: qsun@iue.ac.cn (Q. Sun).

concentrations (Wang et al., 2017). Adsorbents from various categories including zeolites, activated carbon, clay, and ordered mesoporous silica have been reported to remove REEs from the aqueous environment (Qi et al., 2017; Zheng et al., 2015). Although some of these adsorbents show promising performance, most have disadvantages including low adsorption capacity, long equilibrium time, and poor REEs selectivity in complex matrices (Jha et al., 2016; Qiu et al., 2016). The slow adsorption kinetics of REEs is attributed to their large ionic radii and high coordination numbers, which reduce their diffusion rates and limit their ability to access the active sites of the adsorbent (Wang et al., 2017; Zheng et al., 2015). Thus, materials with high removal capacity, fast adsorption kinetics, and high selectivity toward REEs are highly desired.

Polymers of β -cyclodextrin (β -CD), an inexpensive sustainable macrocycle of glucose, have been used as adsorbents for a variety of water purification applications (Alsaiee et al., 2016; Morin-Crini and Crini, 2013). However, the majority of the previously reported β -CD polymers had low surface areas and exhibited very slow adsorption rates toward various classes of water contaminants (Morin-Crini and Crini, 2013). In 2016, Alsaiee et al., reported the first permanently microporous high surface area β -CD polymer, named **P-CDP**, by crosslinking β -CD with the rigid aromatic group tetrafluoroterephthalonitrile. **P-CDP** showed rapid removal of organic micropollutants, Pb ions, and sulfides from water with high adsorption capacities, and it can be easily regenerated at ambient temperature (Alsaiee et al., 2016; Klemes et al., 2018; Li et al., 2017).

Here we examined the ability of **P-CDP** to remove REEs from water using model and industrial wastewater matrices. We also report the synthesis of a magnetic **P-CDP** composite, named herein **P-CDP@Fe₃O₄**, which can be easily isolated by an external magnetic field and it overcomes the clogging and high backpressure issues associated with the use of **P-CDP** while maintaining **P-CDP**'s ability to recover REEs (Alsaiee et al., 2016; Alzate-sanchez et al., 2019). Previous studies reported that the conjugation of magnetic nanomaterials with biopolymers such as cellulose, chitosan, alginate, and cyclodextrin, enable easy isolation of the conjugate from the medium by an external magnetic field, which minimizes the loss of the adsorbent during wastewater treatment (Badruddoza et al., 2013; Reddy and Lee, 2013; Su, 2017). For instance, the magnetic β -cyclodextrin polymers, which are synthesized in three steps, could be easily regenerated while retaining good adsorption performance for organic pollutants and heavy metals in wastewater (Hu et al., 2020; Zhang et al., 2017). **P-CDP@Fe₃O₄** was fully characterized by various structural analysis techniques, and its ability to remove REEs from water was examined. **P-CDP@Fe₃O₄** and **P-CDP** both exhibited fast adsorption and rapid recovery of REEs. Their excellent selectivity for the recovery of REEs from complex industrial wastewaters in the presence of alkali, alkaline earth, and transition metal competitors was also demonstrated. In addition, both adsorbents were fully regenerated multiple times by a simple washing procedure with dilute acidic solutions.

2. Materials and methods

2.1. Reagents and instrumentation

Reagents: β -cyclodextrin (β -CD, >97%), tetrafluoroterephthalonitrile (TFP, >99%), tetrahydrofuran (THF), N,N-dimethylformamide (DMF), Fe₃O₄ nanoparticles (98% metals basis, 20–30 nm), neodymium (III) nitrate hexahydrate (99.9%) [Nd(NO₃)₃·6H₂O], and gadolinium (III) nitrate hexahydrate (99.9%) [Gd(NO₃)₃·6H₂O] were purchased from Sigma–Aldrich (USA). Dichloromethane and K₂CO₃ were purchased from Sinopharm chemical reagent Co. Ltd, Shanghai, China. HCl was obtained from

Merck, while N₂ gas (purity 99.9%) was purchased from Linde Gas, Xiamen, China. A Milli-Q water purification system (Millipore, USA) was used to prepare the deionized water used in this study.

Instrumentation: Infrared (IR) analysis was performed on Thermo Scientific Nicolet iS10, USA. The pore volume, Brunner-Emmett-Teller (BET) specific surface area and Barrett-Joyner-Halenda (BJH) pore size were analyzed by the N₂ adsorption and desorption technique using ASAP 2020 Micrometrics, USA. Thermal gravimetric analysis (TGA) was conducted on Netzsch TG 209 F3 instrument from room temperature to 1000.0 °C under N₂ atmosphere at 10.0 °C/min heating rate. Zeta potential was measured using Nano/submicron particle size analyzer (Zeta PALS, Malvern Instruments, UK). Magnetization studies were conducted using vibrating sample magnetometry (VSM). For the surface morphology, samples were coated with a conductive gold then images were obtained using scanning electron microscopy (SEM, HITACHI S-4800). Particle size analysis was performed using mastersizer 3000 laser diffraction particle size analyzer (Malvern Instruments, UK). REEs concentration in eluents and filtrates were measured using inductively coupled plasma optical emission spectrometry (ICP-OES, PerkinElmer Optima 7000 DV, USA), or inductively coupled plasma mass spectroscopy (ICP-MS, Agilent 7500CX).

2.2. Synthesis of adsorbents

P-CDP was prepared as previously reported, and its synthetic scheme is presented in Fig. S1 (Alsaiee et al., 2016). The synthetic scheme of the magnetic crosslinked β -cyclodextrin composite **P-CDP@Fe₃O₄** is shown in Fig. 1. 0.29 g Fe₃O₄ particles were added to 2.00 g β -CD, 1.00 g TFP, and 3.00 g K₂CO₃ in a round-bottom flask containing 80.0 mL anhydrous THF/DMF (9:1), and the reaction mixture was refluxed under N₂ atmosphere for 48 h at 85 °C. The resulting solid was collected with a magnet and washed with 1.0 M HCl to remove residual K₂CO₃. The solid particles were then washed by immersing in water for 15 min, THF for 30 min, and CH₂Cl₂ for 15 min. **P-CDP@Fe₃O₄** particles were dried under high vacuum at 60 °C for two days.

2.3. Batch adsorption experiments

Since the physical and chemical properties of REEs are similar (Zhang et al., 2016), Nd and Gd were selected as model elements to investigate REEs adsorption on **P-CDP** and **P-CDP@Fe₃O₄**. In general, the adsorption experiments were conducted in an incubator shaker (ZHWY-2102C, China). 500 mg/L stock solutions of Nd and Gd were prepared in Milli-Q water using Nd(NO₃)₃·6H₂O and Gd(NO₃)₃·6H₂O, respectively. The working solutions were prepared by diluting the stock solutions to the desired concentration. The pH values of the working solutions were adjusted using 0.1 mol/L HNO₃ and NaOH solutions. After adsorption, the mixtures were filtrated using 0.45 μ m pore size membrane for **P-CDP** while a permanent Nd–Fe–B magnet was used to isolate **P-CDP@Fe₃O₄**. The residual Nd and Gd concentrations were measured using ICP-OES.

The adsorption kinetic experiments were carried out at a dosage of 1.00 g/L of adsorbent in 250 mL conical flasks containing 100 mL of 5.00 mg/L Nd or Gd solutions at 25 °C, and the flasks are then shaken at 180 rpm. The adsorption isotherm experiments were performed in 20 mL scintillation vials containing 10.0 mg of adsorbents and 10.0 mL of REEs solutions of various concentrations, and the vials were shaken at 180 rpm for 24 h at three different temperatures (25, 35 and 45 °C). The effect of pH on adsorption was studied by adding 1.00 g/L of each adsorbent to 5.00 mg/L solutions of Nd or Gd with initial pH ranging from 1 to 6, and the mixtures

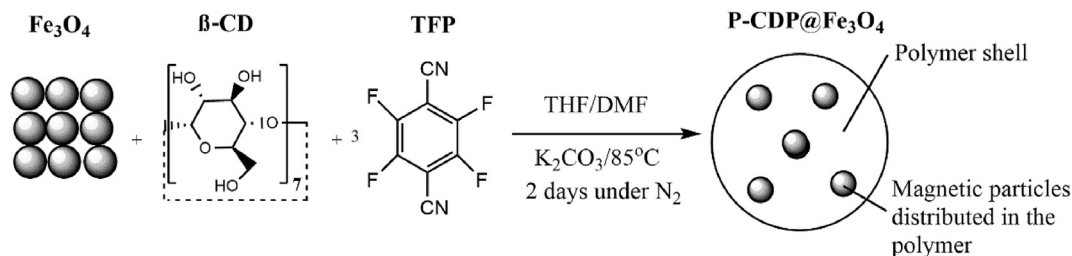


Fig. 1. Synthetic scheme of $\text{P-CDP@Fe}_3\text{O}_4$.

were then shaken at 180 rpm and 25°C for 24 h. After adsorption, the mixtures were filtrated using $0.45\ \mu\text{m}$ pore size membrane for **P-CDP** while a permanent Nd–Fe–B magnet was used to isolate **P-CDP@Fe₃O₄**. The removal efficiency and the amount of adsorbed REEs q_e (mg/g) at equilibrium were calculated according to Eqs. (1) and (2), respectively.

$$\text{Removal efficiency (\%)} = \left(\frac{C_0 - C_t}{C_0} \right) \times 100 \quad (1)$$

$$q_e = \frac{(C_0 - C_t) \times V}{m} \quad (2)$$

Where C_0 and C_t (mg/L) are the initial concentrations and concentrations at time t , V (mL) is the volume of solution, and m (mg) is the mass of the adsorbent.

2.4. Fitting models for kinetic, isotherm and thermodynamic studies

To analyze the adsorption kinetics of REEs, the kinetic experimental data were fitted using pseudo-first-order and pseudo-second-order as Eqs. (3) and (4), respectively (Ho and McKay, 1999; Lagergren, 1898)

$$\text{Pseudo – first – order kinetic model: } \ln(q_e - q_t) = \ln q_e - k_1 t \quad (3)$$

$$\text{Pseudo – second – order kinetic model: } \frac{t}{q_t} = \frac{1}{q_e} t + \frac{1}{k_2 q_e^2} \quad (4)$$

where k_1 (1/min) and k_2 (g/mg min) are the rate constants of the pseudo-first-order and pseudo-second-order models, respectively. q_e (mg/g) and q_t (mg/g) are the amounts of adsorbed REEs at equilibrium and time t , respectively.

The adsorption isotherm studies were fitted by Langmuir and Freundlich models, which are expressed in Eq. (5) and Eq. 6, respectively (Freundlich, 1907; Langmuir, 1918)

$$\frac{C_e}{q_e} = \frac{1}{q_m} C_e + \frac{1}{q_m K_L} \quad (5)$$

$$\ln q_e = \frac{1}{n} \ln C_e + \ln K_F \quad (6)$$

where q_e (mg/g) is the amount of adsorbate adsorbed per mass of adsorbent at equilibrium, C_e (mg/L) is the equilibrium concentration of adsorbate in aqueous solution, q_m (mg/g) is the monolayer adsorption capacity at equilibrium, K_L is the Langmuir equilibrium constant, K_F and n are Freundlich constants for a given adsorbent and adsorbate at certain temperature.

The thermodynamic parameters are calculated according to the

laws of thermodynamics using the following equations

$$\Delta G^\circ = -RT \ln K_c \quad (7)$$

$$\ln K_c = -\frac{\Delta H^\circ}{R} \times \frac{1}{T} + \frac{\Delta S^\circ}{R} \quad (8)$$

$$K_c = 55.5 \times 1000 \times K_L \quad (9)$$

where R is the universal gas constant (8.3144 J/mol K), and T is the absolute temperature in Kelvin. K_c is the equilibrium constant (dimensionless) derived from the Langmuir constant (K_L), while the factor 55.5 is the number of moles of pure water per liter (1000 g/L divided by 18 g/mol) (Tran et al., 2017, 2016).

2.5. Competitive adsorption experiments

To study adsorption selectivity of **P-CDP** and **P-CDP@Fe₃O₄** toward REEs, competitive adsorption experiments were carried out in a 50 mL conical flask by mixing 20.0 mg of adsorbent with 10.0 mL solution containing Y, Nd, Eu, Gd, Na, Ca, Mg, Ni, and Zn with initial concentrations of 5.00 mg/L, then shaking the mixture at 25°C for 24 h. The mixtures were then filtrated using $0.45\ \mu\text{m}$ pore size membrane for **P-CDP** while a permanent Nd–Fe–B magnet was used to isolate **P-CDP@Fe₃O₄**. After determining the concentrations of the residual REEs by ICP-OES, the distribution coefficients (K_d , mL/g) of the metal ions were calculated using Eq. (10)

$$K_d = \left(\frac{C_0 - C_f}{C_f} \right) \times \frac{V}{m} \quad (10)$$

where C_0 and C_f (mg/L) are the initial and final concentration of the metal ion, respectively, and V and m are the volume of solution and adsorbent mass, respectively.

2.6. Adsorbent reusability studies

Reusability studies were conducted using solid-phase extraction (SPE) method, in which 2.5 mL empty SPE cartridges were packed with 100 mg of **P-CDP** or **P-CDP@Fe₃O₄** and then connected to Visiprep SPE vacuum manifold (Supelco). Before loading the sample, the cartridges were washed with Milli-Q water (10 mL). Then 10.0 mL Nd or Gd (5.00 mg/L, pH 5.0) solutions were passed through the cartridges at a controlled flow rate of 0.5 mL/min for **P-CDP** and 3 mL/min for **P-CDP@Fe₃O₄**. The filtrates were then collected and analyzed using ICP-OES. To regenerate the adsorbent and recover the metal ions, 0.5 M HNO_3 or 0.5 M HCl were passed through the cartridges at a flow rate of 0.5 mL/min for **P-CDP** and 3 mL/min for **P-CDP@Fe₃O₄**. The residual Nd or Gd in the acidic filtrates were then analyzed by ICP-OES. The above procedure was repeated five times. The recovery efficiency of Nd and Gd was calculated using Eq. (11) (Wang et al., 2017).

$$\text{Recovery efficiency (\%)} = \frac{C_{des}}{C_o} \times 100 \quad (11)$$

where C_{des} and C_o (mg/L) are the metals concentration before adsorption and after desorption, respectively.

2.7. Adsorption studies with industrial wastewater

A wastewater sample from a local REEs processing industry was diluted 100 times to prepare a working wastewater solution, and the pH of the working solution was adjusted to 5.0 using 1 mol/L HNO_3 and NaOH solutions. 10.0 mL working solution was then mixed with 30.0 mg adsorbent in 50 mL conical flask and shaken for 20 min at 25 °C. The mixture was then filtrated using 0.45 μm pore size membrane for **P-CDP** while a permanent Nd–Fe–B magnet was used to isolate **P-CDP@Fe₃O₄**. The solids were then washed one time with deionized water, and then the adsorbed ions were eluted using 0.5 M HNO_3 . The ions in the acidic filtrates were analyzed by ICP-MS to determine the concentration of the desorbed ions.

3. Results and discussion

3.1. Characterization of the adsorbents

3.1.1. FT-IR analysis

FT-IR spectra of β -CD, TFP, **P-CDP**, Fe_3O_4 , and **P-CDP@Fe₃O₄** are shown in Fig. 2A. For β -CD and Fe_3O_4 , the intense and broad peak around 3419 cm^{-1} belongs to –OH stretching vibrations (Nkinahamira et al., 2017) and the bands at 1645 cm^{-1} and 1450 cm^{-1} are associated with the C–C aromatic stretches. The band at 2931 cm^{-1} in the spectra of β -CD and TFP is assigned to the aliphatic C–H stretches, while the band at 1033 cm^{-1} in the spectrum of β -CD corresponds to the C–O stretch (Alsbaiee et al., 2016). The bands at 2244 cm^{-1} and 1271 cm^{-1} in the spectra of **P-CDP** and **P-CDP@Fe₃O₄** belong to the C–F and nitrile groups, respectively. The presence of the band at 594 cm^{-1} in the IR spectrum of **P-CDP@Fe₃O₄** is attributed to the Fe–O bonds in the Fe_3O_4 particles (Badruddoza et al., 2013).

3.1.2. Thermal stability

The TGA analyses of the monomers and polymers are shown in Fig. 2B. The TGA curve of Fe_3O_4 showed a weight loss of 3.44% over the full temperature range, which can be attributed to the removal of physisorbed water and surface OH groups due to the oxidation of iron (Abdolmaleki et al., 2015). **P-CDP** and **P-CDP@Fe₃O₄** showed enhanced thermal stability as compared with TFP and β -CD. The initial weight drop of 3.95% and 4.40% for **P-CDP** and **P-CDP@Fe₃O₄**, respectively, occurred between 40 and 263 °C, which is attributed to the evaporation of physically absorbed water (Nkinahamira et al., 2017). The weight loss of 31.97% for **P-CDP** and 23.09% for **P-CDP@Fe₃O₄** that occurred between 263 and 383 °C is attributed to the decomposition of TFP, whereas the weight loss after 383 °C in both materials is attributed to the degradation of β -CD (Tsiepe et al., 2018). The weight drop of 11.93% for **P-CDP@Fe₃O₄** between 625 and 666 °C, which is absent in **P-CDP**, could be attributed to the oxidation of Fe_3O_4 to Fe_2O_3 , which may further indicate the successful incorporation of the Fe_3O_4 particles in **P-CDP@Fe₃O₄** (Abdolmaleki et al., 2015).

3.1.3. Zeta potential

The charge of a material's surface in solution is characterized by the isoelectric point (IEP) or the point of zero charge (PZC) (Tran et al., 2017). Zeta potentials of **P-CDP** and **P-CDP@Fe₃O₄** are

shown in Fig. 2C. Both materials have negative zeta potential values in acidic and basic solutions with PZC at pH 5.3 for **P-CDP** and PZC at pH 4.1 for **P-CDP@Fe₃O₄**, which can be attributed to the presence of the phenolate groups in both materials as reported previously (Klemes et al., 2018). The lower PZC of **P-CDP@Fe₃O₄** as compared with **P-CDP** might be due to its higher oxygen content (Faria et al., 2004) as shown in Fig. S2. It should be pointed out that the negative zeta potentials of both adsorbents are advantageous for the adsorption of positively charged REE ions, and it reduces the tendency of both materials to agglomerate in solution (Yirsaw et al., 2016).

3.1.4. Magnetization measurements

VSM was used to measure the magnetization values of Fe_3O_4 and **P-CDP@Fe₃O₄** at room temperature, and the results are shown in Fig. 2D. The hysteresis loops of Fe_3O_4 and **P-CDP@Fe₃O₄** indicate their ferromagnetic behavior with magnetic saturation of 66 and 16 emu/g, respectively. The low magnetization value of **P-CDP@Fe₃O₄** can be attributed to the existence of nonmagnetic material layer (i.e. **P-CDP**) in the composite and the decrease of the weight percent of Fe_3O_4 in the composite as compared with the neat Fe_3O_4 (Qiu et al., 2016). Nevertheless, **P-CDP@Fe₃O₄** exhibited strong magnetic responsiveness and can be separated easily from solution using an external magnet (Li et al., 2006).

3.1.5. Porosity and surface area analyses

Porosity and surface area of the adsorbents and their corresponding monomers were investigated by ASAP nitrogen porosimetry analysis. Fe_3O_4 nanoparticles showed type-III isotherms with BET surface area of 73 m^2/g , pore volume of 0.240 cm^3/g and pore size of 13.1 nm (Fig. 3A). **P-CDP** and **P-CDP@Fe₃O₄** exhibited type-II isotherms (Fig. 3B and C) characteristic of mesoporous materials as supported by the BJH pore size distribution curves (Fig. 3D) with an average pore size of 2.88 nm and 4.81 nm, respectively. Notably, the BET surface area of **P-CDP@Fe₃O₄** was 85 m^2/g as compared with a surface area of 143 m^2/g for **P-CDP**, which can be attributed to the incorporation of the Fe_3O_4 particles in **P-CDP@Fe₃O₄** (Nkinahamira et al., 2017).

3.1.6. Morphology and elemental analysis

SEM images of Fe_3O_4 (Fig. 4A) revealed agglomerations of small spherical particles, whereas the SEM images of **P-CDP** (Fig. 4B) showed irregular shape and size particles with rough surfaces indicative of the porous structure of **P-CDP**. The SEM images of **P-CDP@Fe₃O₄** (Fig. 4C) relatively resembled those of **P-CDP** but seemed to have smaller particle size. The average particle size measured using laser diffraction particle size analyzer was found to be 116 μm and 25.3 μm for **P-CDP** and **P-CDP@Fe₃O₄**, respectively. A further evidence of the presence of Fe_3O_4 particles in **P-CDP@Fe₃O₄** is provided by the EDX analysis (Fig. 4D) which indicated the presence of 29.8 wt% Fe (9.56 mol% Fe) in the composition of **P-CDP@Fe₃O₄**. EDX data for β -CD, TFP, **P-CDP**, and Fe_3O_4 were given in Fig. S2.

3.2. Results of batch experiments

3.2.1. Effect of pH

The effect of pH on Nd and Gd adsorption by **P-CDP** and **P-CDP@Fe₃O₄** was investigated at pH 2–6 for Nd and 2–5.5 for Gd. As shown in Fig. 5 A and B, the adsorption process was strongly dependent on solution pH, in that, the removal capacity of Nd and Gd increased with increasing pH from 2 to 5.5. Since both adsorbents have negative zeta potentials (Fig. 2C), the low removal efficiency in the stronger acidic conditions can be attributed to the competition between H^+ and the metal ions as was reported

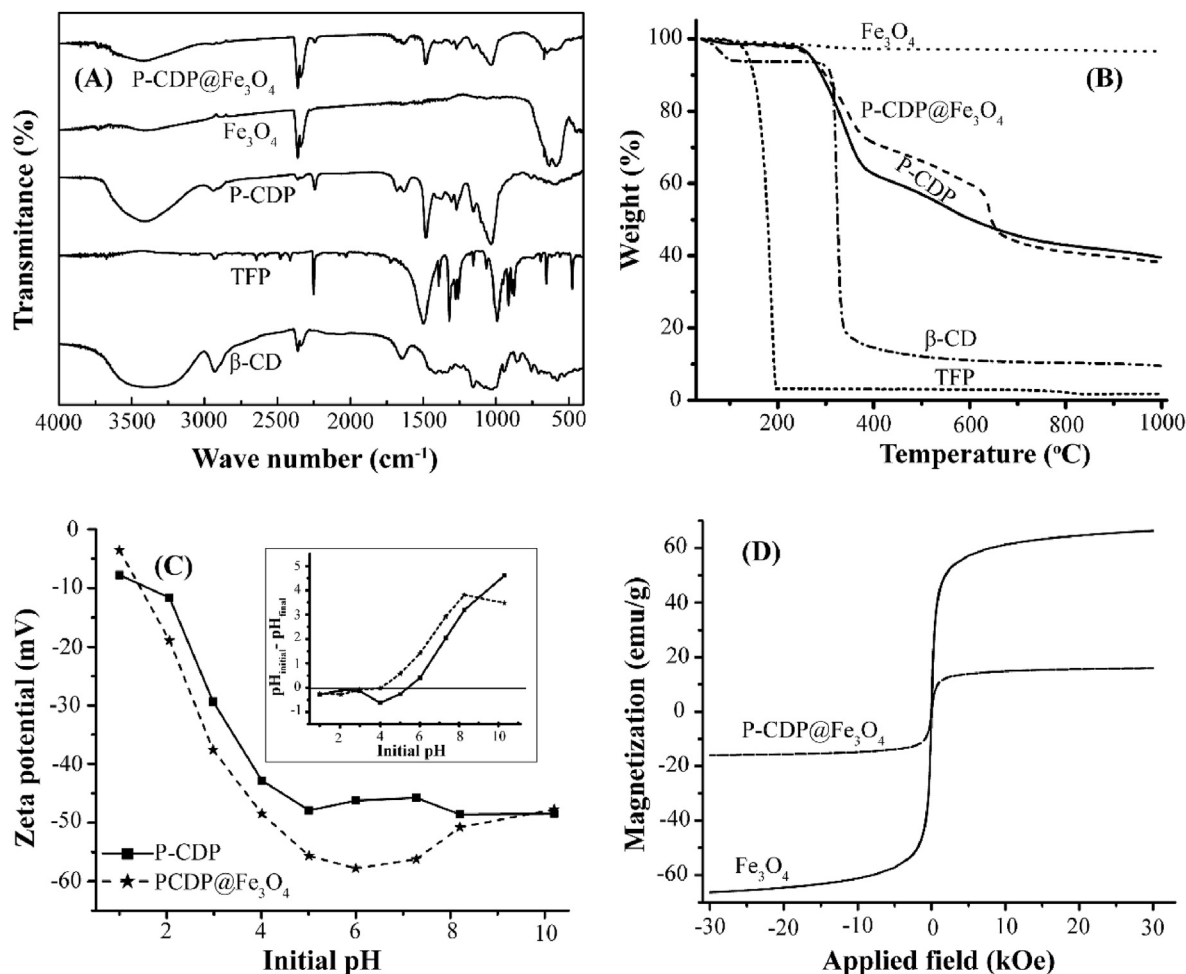


Fig. 2. (A) FT-IR spectra, (B) TGA (heated with the rate of 10 °C/min up to 1000 °C under nitrogen) for β -CD, TFP, P-CDP, Fe_3O_4 , and P-CDP@ Fe_3O_4 , (C) zeta potentials (inset figure shows the point of zero charge) for P-CDP and P-CDP@ Fe_3O_4 , (D) hysteresis loops of Fe_3O_4 and P-CDP@ Fe_3O_4

previously (Zhu et al., 2011). Therefore, both Nd and Gd exhibited maximum removal efficiency in the pH range of 5–5.5. For instance, the maximum removal efficiencies were 93% (Nd) and 77% (Gd) by P-CDP, and 94% (Nd) and 72% (Gd) by P-CDP@ Fe_3O_4 .

3.2.2. Effects of contact time and adsorption kinetics

Fig. 5C and D shows the adsorption of Nd and Gd on P-CDP and P-CDP@ Fe_3O_4 as a function of time. In less than 5 min, both adsorbents achieved 90% removal and nearly 100% adsorption after approximately 10 min. This rapid removal of REEs is attributed to the high surface area and porosity of P-CDP and P-CDP@ Fe_3O_4 , which is consistent with previous studies that reported rapid adsorption of micropollutants on P-CDP (Alsbaiee et al., 2016). According to the kinetic parameters calculated using Eqs. (3) and (4) and shown in Table S1 and Fig. S3, the adsorption of Nd and Gd fitted well the pseudo-second-order kinetic model with correlation coefficients (R^2) greater than 0.998 similar to previously reported β -CD polymers (Abdolmaleki et al., 2015; Alzate-sanchez et al., 2019; Morin-Crini and Crini, 2013).

3.2.3. Adsorption isotherm and capacity

Adsorption isotherms of Nd and Gd are shown in Fig. 5 E and F. The adsorption capacities of P-CDP and P-CDP@ Fe_3O_4 increased with the initial concentration of Nd and Gd then reached

equilibrium. The experimental isotherm data were fitted by Langmuir and Freundlich models according to Eqs. 5 and 6, respectively. The parameters associated with Langmuir and Freundlich models are presented in Table 1. Based on the correlation coefficient value (R^2) and the inset in Fig. 5 E and F, the adsorption of Nd and Gd better fitted the Langmuir model (Langmuir, 1918).

Based on Langmuir isotherm data in Table 1, the maximum adsorption capacities of Nd and Gd on P-CDP were 9.59 and 8.99 mg/g, respectively. While, the maximum adsorption capacities on P-CDP@ Fe_3O_4 were 8.88 and 7.76 mg/g, respectively (initial concentration ranging from 1 to 100 mg/L). The slightly lower adsorption capacity of P-CDP@ Fe_3O_4 as compared with P-CDP is attributed to the lower weight percentage of the β -CD polymer in the composite. Since the adsorption fitted the Langmuir model, it is essential to calculate the separation factor (R_L), which is a dimensionless constant that determines whether the adsorption is favorable ($R_L < 1$) or unfavorable ($R_L > 1$) and can be calculated using Eq. (12) (Weber and Chakravorti, 1974).

$$R_L = \frac{1}{1 + K_L C_0} \quad (12)$$

Where R_L is a constant separation factor (dimensionless) of the solid-liquid adsorption system, K_L is the Langmuir equilibrium

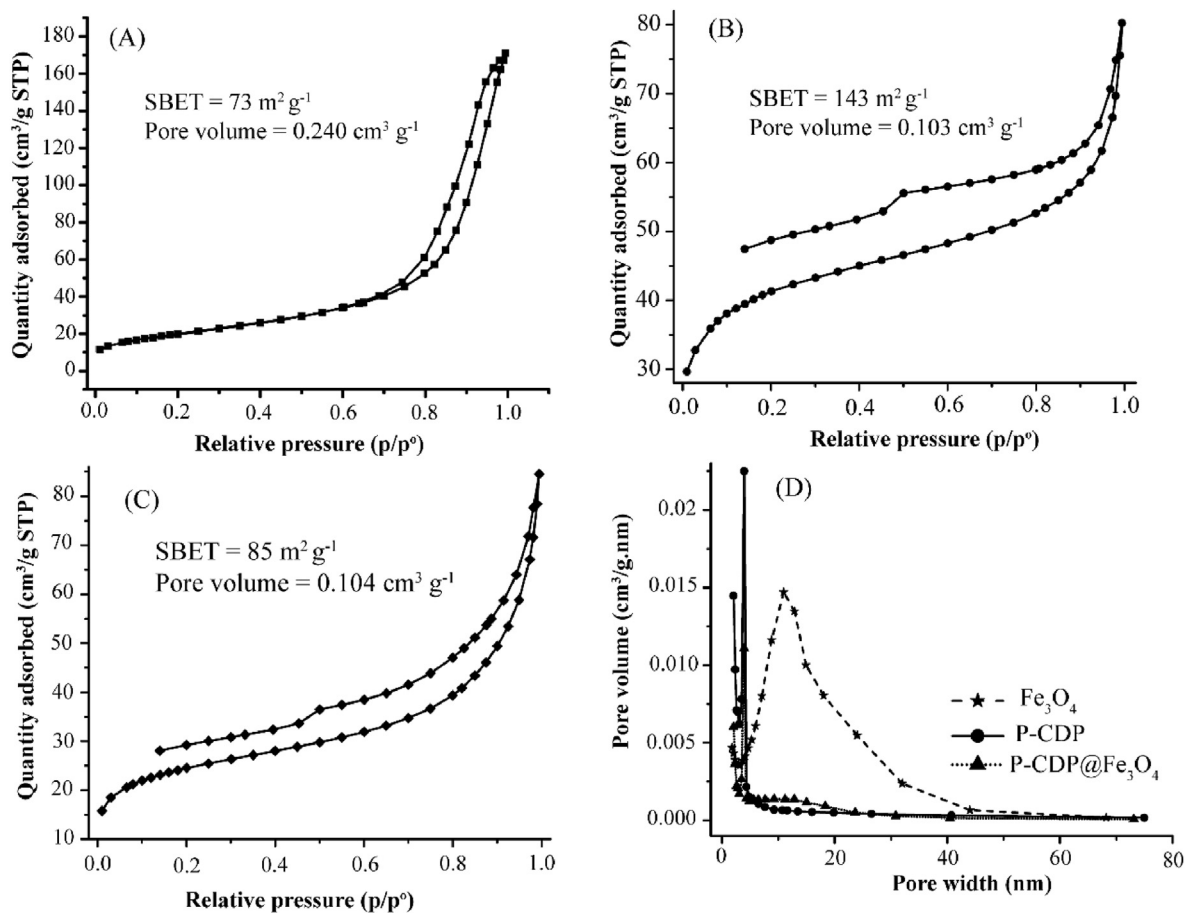


Fig. 3. Nitrogen adsorption-desorption isotherms at 77 K for (A) Fe_3O_4 , (B) P-CDP, (C) P-CDP@ Fe_3O_4 , and (D) pore-size distribution curve.

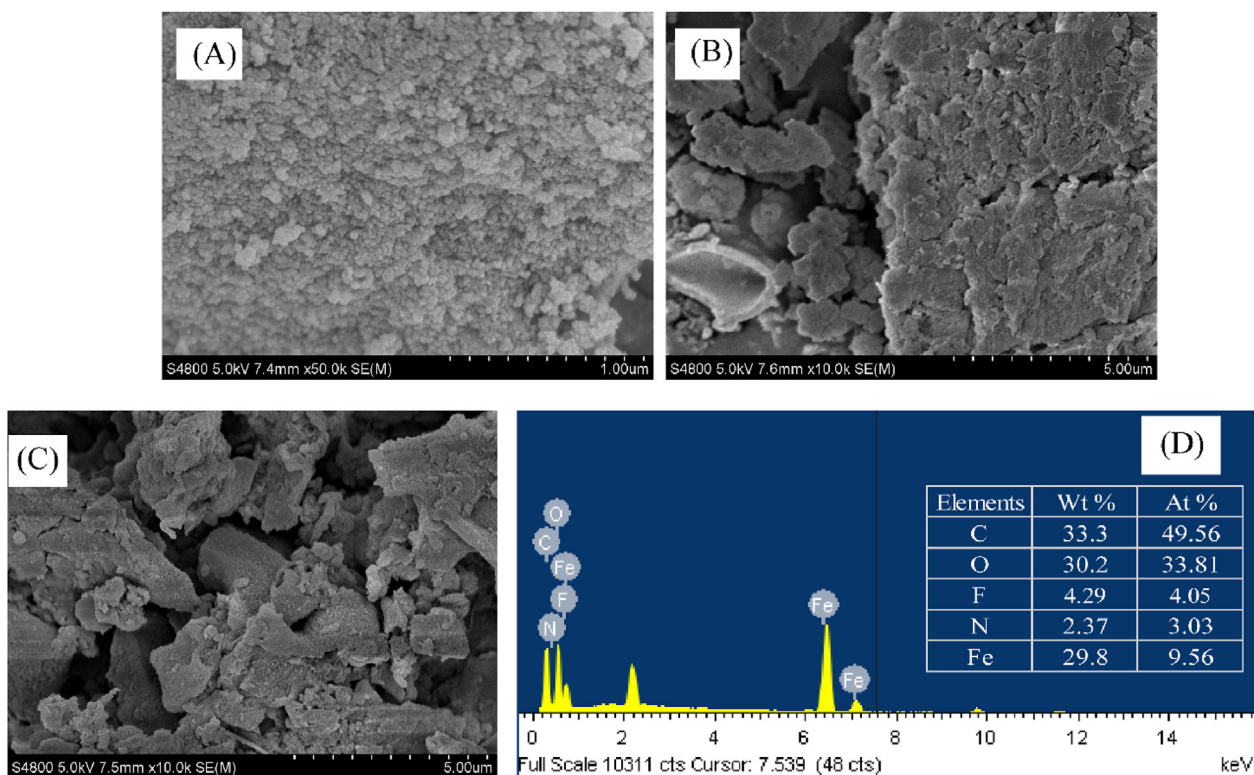


Fig. 4. SEM images of (A) Fe_3O_4 , (B) P-CDP, (C) P-CDP@ Fe_3O_4 , and (D) EDX analysis for P-CDP@ Fe_3O_4

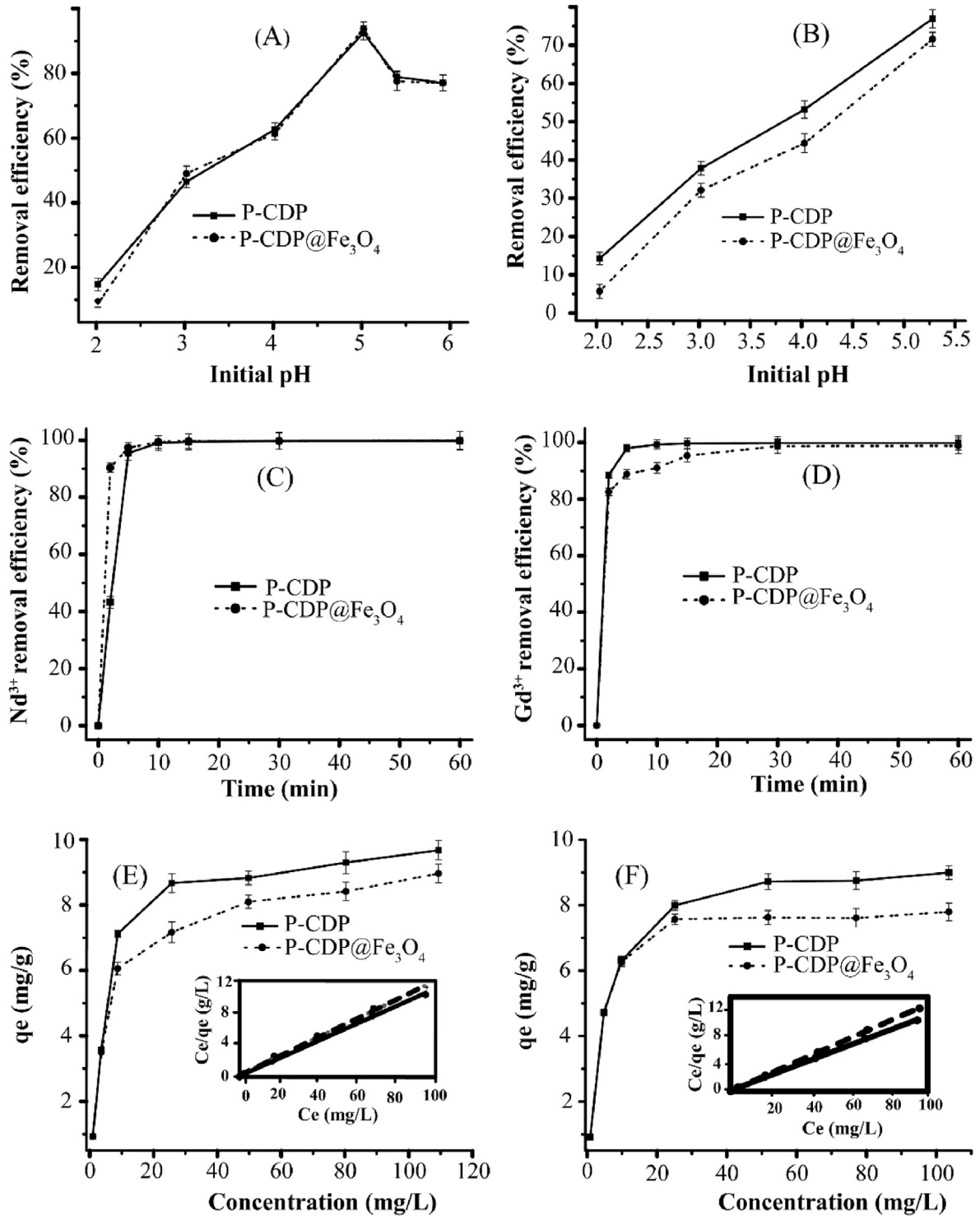


Fig. 5. Effect of solution pH on adsorption of (A) Nd and (B) Gd (adsorbent dose: 1.00 g/L, initial concentration: 5.00 mg/L, temperature: 25 °C), adsorption kinetics of (C) Nd, (D) Gd (pH: 5, adsorbent dose: 1.00 g/L, initial concentration: 5.00 mg/L, temperature: 25 °C). Adsorption isotherms of (E) Nd, and (F) Gd (adsorbent dose: 1.00 g/L, contact time: 24 h, pH: 5.0, temperature: 25 °C). The inset of (E) and (F) are the Langmuir isotherms of adsorption. Error bars represent the maximum and minimum values for two replicate experiments.

constant, and C_0 (mg/L) is the initial adsorbate concentration.

As shown in Table 1, the values of R_L ranged between 0 and 1, and the concave shape of the adsorption isotherm indicated that REEs adsorption by P-CDP and P-CDP@Fe₃O₄ was favorable (Tran et al., 2017).

3.2.4. Adsorption thermodynamic parameters and adsorption mechanism

Calculation of adsorption thermodynamic parameters is fundamental to understand the adsorption mechanism. Gibbs free energy (ΔG°) was calculated using Eq. (7), and the enthalpy (ΔH°)

Table 1
Parameters of Langmuir and Freundlich adsorption isotherm models.

Adsorbents	REEs	Langmuir parameters				Freundlich parameters			
		q_m (mg/g)	K_L (L/mg)	R_L	R^2	n	k_F (mg/g.(L/mg) ^{1/n})	R^2	
P-CDP	Nd	9.59	0.96	0.01-0.53	0.999	4.87	4.43	0.831	
	Gd	8.99	1.00	0.01-0.52	0.999	4.96	4.24	0.840	
P-CDP@Fe ₃ O ₄	Nd	8.88	0.55	0.17-0.66	0.997	4.20	3.49	0.863	
	Gd	7.76	2.15	0.00-0.337	1.000	5.29	3.97	0.782	

Table 2
Thermodynamic parameters of the adsorption of Nd and Gd on P-CDP and P-CDP@Fe₃O₄

Adsorbents	REEs	T (°C)	ΔG° (kJ/mol)	ΔH° (kJ/mol)	ΔS° (J/mol K)	R^2
P-CDP	Nd	25	-25.57	49.65	252.75	0.986
		35	-28.42			
		45	-30.61			
	Gd	25	-27.10	9.74	123.58	0.991
		35	-28.35			
		45	-29.54			
P-CDP@Fe ₃ O ₄	Nd	25	-25.57	32.74	196.00	0.969
		35	-27.85			
		45	-29.47			
	Gd	25	-28.96	19.85	163.72	0.997
		35	-30.54			
		45	-32.24			

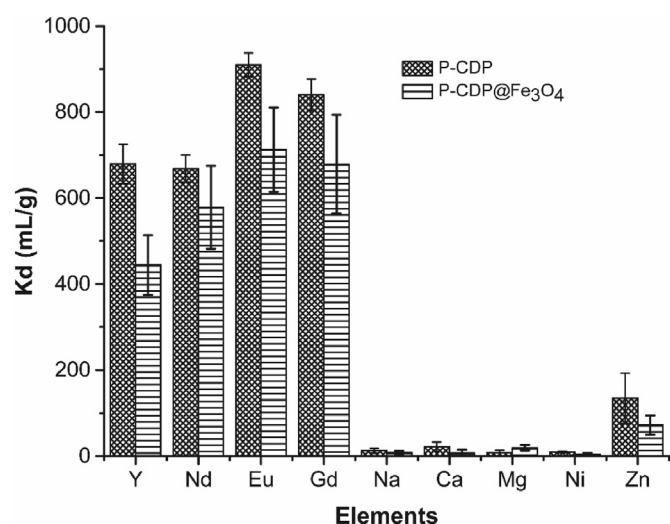


Fig. 6. Distribution coefficients (K_d) of adsorption of REEs and various competitive ions in a model solution containing mixtures of these metal ions (pH: 5, adsorbent dose: 2.0 g/L, initial concentration: 5.00 mg/L, temperature: 25 °C). Error bars show the standard deviations for three replicate experiments.

and entropy (ΔS°) components were determined from the slope and intercept, respectively, of the plot of $\ln K_c$ versus $1/T$ in van't Hoff equation Eq. (8) as shown in Fig. S4. The values of these thermodynamic parameters are summarized in Table 2. The positive values of ΔH° indicate that Nd and Gd must replace more than one water molecule upon their adsorption on P-CDP and P-CDP@Fe₃O₄, which causes the endothermicity of the adsorption process affirming a chemisorption process (Saha and Chowdhury, 2011). Overall, the increase of the negative values of ΔG° with temperature indicates that the adsorption process is spontaneous and that it becomes more favorable at high temperature. Possibly increasing temperature increases the mobility of Nd and Gd in solution, which increases their affinity on the adsorbents (Saha and Chowdhury, 2011; Tran et al., 2016). Additionally, since ΔG° values are all below -20 kJ/mol, the adsorption process is likely to

be dominated by chemisorption according to previous reports (Anastopoulos et al., 2016). In the chemisorption process, REEs can form coordination complexes with donor atoms including oxygen, nitrogen, and fluorine in P-CDP and P-CDP@Fe₃O₄ (Hasegawa et al., 2011; Pearson, 1968). In addition, electrostatic interactions between the negatively charged phenolate groups in the adsorbents and the adsorbed REEs ions are very likely to occur based on a previous report (Klemes et al., 2018), and based on our findings here that the adsorption capacity is increased with increasing pH (Tran et al., 2016).

3.2.5. Selectivity toward REEs

REEs occur in complex matrices, which contain considerable amounts of alkali, alkaline earth, and heavy metals (Zhu et al., 2011). Therefore, it is critical to study the matrix effect on the performance of P-CDP and P-CDP@Fe₃O₄. Fig. 6 shows the distribution coefficients (K_d) of Y, Nd, Eu, and Gd in a mixture containing Na, Ca, Mg, Ni, and Zn with initial concentrations of 5.00 mg/L. The distribution coefficients of REEs and the competitive elements were calculated using Eq. (10), and the separation factors (SF) were calculated from the ratios of the distribution coefficients (Callura et al., 2018). P-CDP and P-CDP@Fe₃O₄ adsorbed much more Y, Nd, Eu, and Gd than the background metals. For example, the SFs of Gd³⁺ versus Na, Ca, Mg, Ni, and Zn were 67.69, 38.93, 115.9, 87.76, and 6.260 in P-CDP and 80.78, 98.98, 35.55, 171.2, and 9.387 in P-CDP@Fe₃O₄, respectively. The SFs of Nd versus the other competitive elements are shown in Table S2. This high selectivity toward REEs can be explained by the Hard and Soft Acids and Bases (HSAB) principle since REEs are hard Lewis acids and P-CDP and P-CDP@Fe₃O₄ contain the hard Lewis base atoms O, N, and F (Pearson, 1968).

3.2.6. Desorption and reusability

In addition to the fast kinetics, good capacity, and high selectivity, P-CDP and P-CDP@Fe₃O₄ can be regenerated multiple times by a simple washing procedure with dilute acidic solution. The reusability of both materials was assessed for five consecutive cycles by saturating with 5.00 mg/L solutions of Nd and Gd, and then desorption with 0.5 M HNO₃. Notably, the backpressure of P-CDP

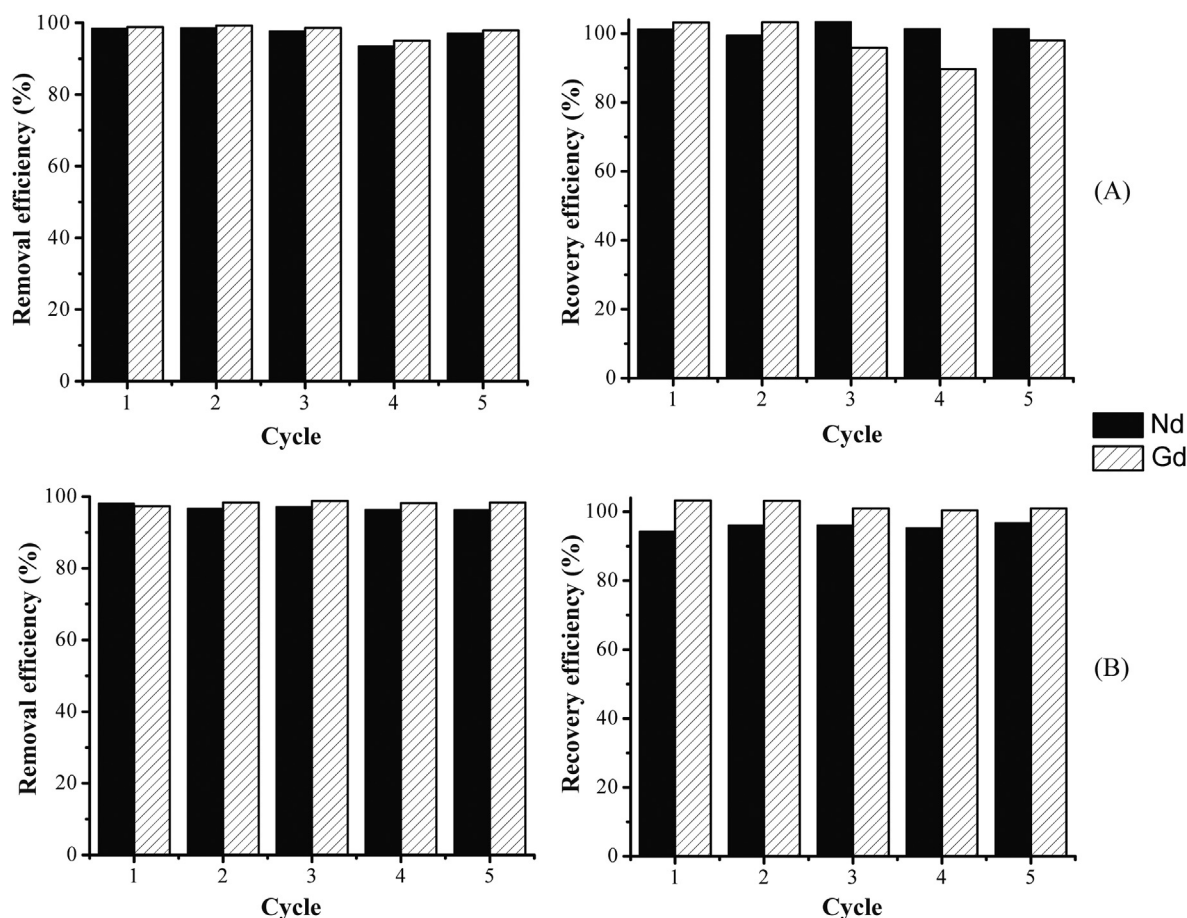


Fig. 7. Removal efficiencies (%) and recovery efficiencies (%) of Nd and Gd for five adsorption-desorption cycles by (A) P-CDP and (B) P-CDP@Fe₃O₄, using 0.5 M HNO₃ as eluent.

Table 3

Elemental composition of diluted industrial wastewater sample.

REEs (μg/L)		Competitive elements (μg/L)	
Y	387.81	Na	1405.8
La	149.35	Mg	2127.7
Ce	3.6922	Ca	20516
Pr	0.86430	Co	2.3873
Nd	12.602	Ga	1033.2
Sm	1.1662	Rb	9.1004
Eu	10.615	Sr	251.83
Gd	19.080	Cs	0.69424
Dy	6.2022	Ba	7329.0
Ho	460.24	Nb	0.85552
Er	365.31	Sn	1.7105
Tm	50.154		
Yb	199.11		

was higher than that of P-CDP@Fe₃O₄ due to the larger particle size of the later, and therefore, the flow rates of the adsorbates and eluents were set at 0.5 mL/min and 3 mL/min for P-CDP and P-CDP@Fe₃O₄, respectively. The removal efficiencies and recovery efficiencies of both REEs were calculated using Eqs. (1) and (11), and the results are shown in Fig. 7. After the fifth cycle, the removal efficiencies of Nd and Gd by P-CDP and P-CDP@Fe₃O₄ remained above 97%. The recovery efficiencies of both ions by both adsorbents after five cycles were above 96%. Other dilute acidic eluents such as 0.5 M HCl were also used and similar results were obtained (Fig. S5).

3.2.7. Application to industrial wastewater

The recovery of REEs from a wastewater sample obtained from a local REEs processing industry using P-CDP and P-CDP@Fe₃O₄, was also investigated to demonstrate the adsorbents performance under realistic environmental conditions. The wastewater sample contained various REEs and competitive metal ions as shown in Table 3. Batch adsorption experiments (contact time 20 min at ambient temperature) indicated that the distribution coefficients (K_d) of REEs on P-CDP and P-CDP@Fe₃O₄ ranged from 413.7 to 1646 mL/g and 304.0–1483 mL/g, respectively, whereas the K_d of the competitive metals on P-CDP and P-CDP@Fe₃O₄ ranged from

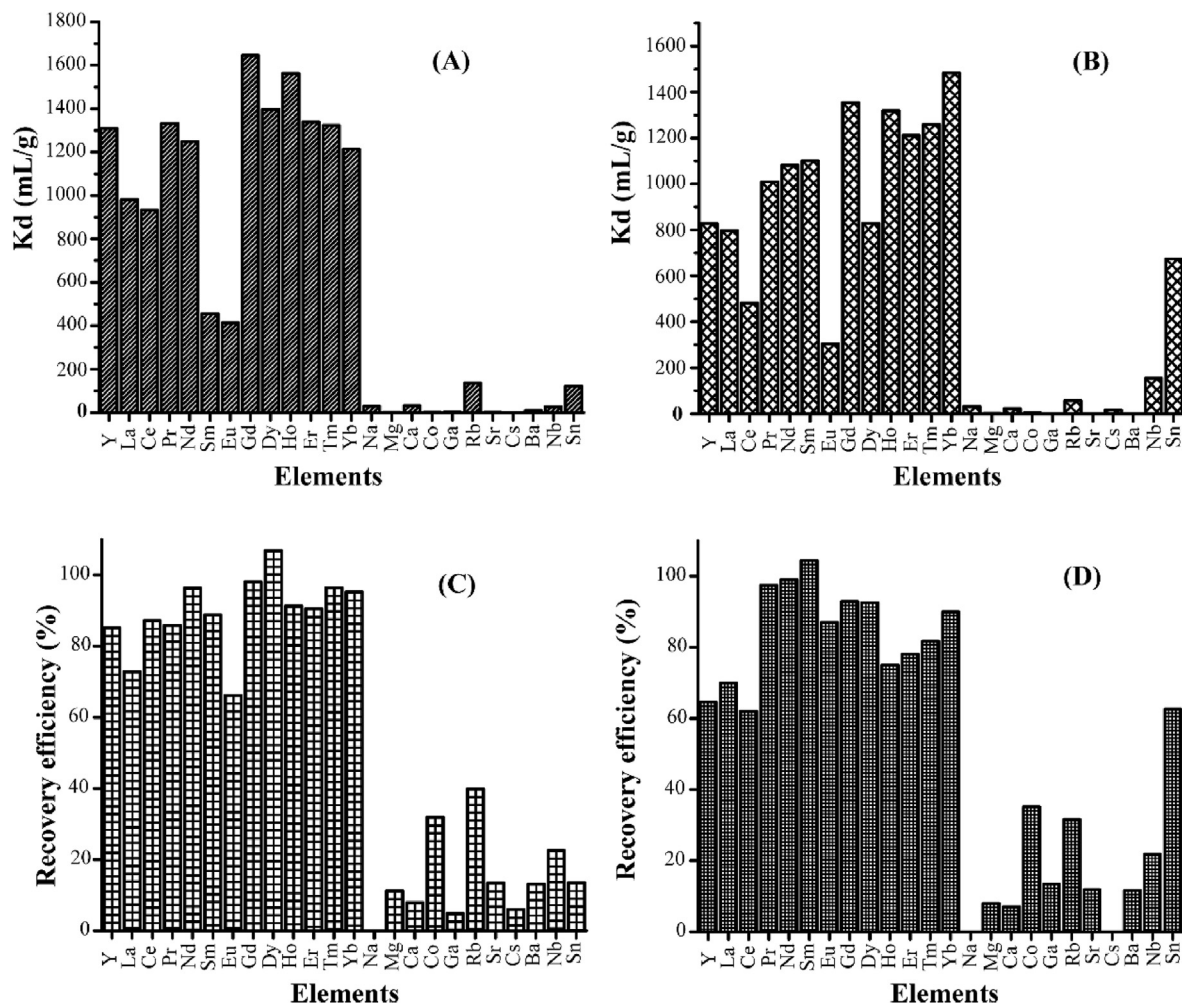


Fig. 8. The adsorption selectivity of REEs in industrial wastewater. (A) and (B) plots show the distribution coefficients (K_d) of REEs and the competitive metal ions on P-CDP and P-CDP@Fe₃O₄, respectively, whereas (C) and (D) plots show the recovery efficiency of REEs and the competitive ions on P-CDP and P-CDP@Fe₃O₄, respectively.

0.4026 to 136.4 mL/g and 0.1820–674.8 mL/g, respectively, as shown in Fig. 8A and B. The apparent higher K_d values of REEs compared with those of the competitive metals confirmed the good selectivity of both adsorbents toward REEs. In addition, the recovery efficiencies of REEs by both adsorbents were in the range of 62%–107% (Fig. 8).

3.3. Environmental implication

Recovery of REEs from industrial wastewater is one of the major challenges in water purification industry. Contamination with REEs raised concerns due to their potential negative health effects and environmental toxicity (Gwenzi et al., 2018; Pagano et al., 2016). Various adsorbent materials have been reported to sequester REEs from wastewater, but these adsorbents suffer from slow adsorption kinetics, poor reusability, and high cost (Anastopoulos et al., 2016; Zheng et al., 2015). Recently, an inexpensive porous polymer of β -CD, namely P-CDP, showed promise for the rapid removal of organic contaminants from water (Alsbaiee et al., 2016). Here we developed a magnetic composite of P-CDP, namely P-CDP@Fe₃O₄, and examined the ability of both P-CDP and P-CDP@Fe₃O₄ to recover REEs from industrial wastewater. These adsorbents show several favorable environmental implications for this application. They can rapidly remove REEs such as Nd and Gd in less than

10 min, which was faster than most previously reported adsorbents, and they display excellent selectivity toward REEs in the presence of several other competitive metal ions. Although some adsorbents such as chitosan-silica composite, β -CD/magnetic attapulgite, calcium alginate and MNSP-N-2 showed higher adsorption capacity toward REEs, adsorbents in this study demonstrated faster equilibrium time (Anastopoulos et al., 2016; Zheng et al., 2015; Guo et al., 2015). In addition, the cost-effective monomers (one of which is sustainable and bio-mass derived), one-step preparation, and simple reuse at ambient temperature, indicate their economic competitiveness and potentially low environmental impact. Furthermore, the incorporation of Fe₃O₄ particles in P-CDP@Fe₃O₄ facilitated the synthesis, application, and regeneration of P-CDP while maintaining its ability in the rapid, selective, and efficient recovery of REEs. Thus, the magnetic composite P-CDP@Fe₃O₄ may potentially further reduce the cost associated with the production, use, and reuse of P-CDP.

4. Conclusions

A magnetic composite of the porous β -CD polymer P-CDP, namely P-CDP@Fe₃O₄, was developed in one synthetic step. P-CDP@Fe₃O₄ has a BET surface area of 85 m²/g and similar microporous structure to P-CDP. The incorporation of the magnetic Fe₃O₄

particles in **P-CDP@Fe₃O₄** reduced the clogging and high back-pressure issues of **P-CDP** and enabled much easier isolation of the adsorbent particles by an external magnet, which facilitated its synthesis and use for water purification. The use of **P-CDP** and **P-CDP@Fe₃O₄** for the recovery of REEs (e.g., Nd, Gd, Y, Eu) from water was examined. Both adsorbents were found to fit a pseudo-second order kinetic model and achieve equilibrium uptake in less than 10 min. The thermodynamic studies of adsorption fitted the Langmuir isotherm model, with adsorption capacities q_{max} of 9.59 mg/g (Nd) and 8.99 mg/g (Gd) on **P-CDP** and 8.88 mg/g (Nd) and 7.76 mg/g (Gd) on **P-CDP@Fe₃O₄** with the highest initial concentration of 100 mg/L. More importantly, both adsorbents exhibited excellent selectivity toward REEs in the presence of various competitive alkali, alkaline earth, and heavy metal ions, both in the model studies and industrial wastewater. The recovery efficiencies of REEs from industrial wastewater using both adsorbents ranged from 62% to 100%. In addition, both adsorbents were reused for five cycles using a simple washing procedure with dilute acidic solutions. These characteristics make **P-CDP** and **P-CDP@Fe₃O₄** promising candidates for REEs sequestration and recovery.

Declaration of competing interest

The authors declare the following financial interests/personal relationships which may be considered as potential competing interests: Alaaeddin Alsaiee is employed by DuPont in its Electronics & Imaging business unit. DuPont also has a Water Solutions business unit in its Safety & Construction business, which offers products for ion exchange and other water purification materials.

Acknowledgments

For financial support, the authors are grateful to the FJRISM&IUE Joint Research Fund (No. RHZX-2018-005), Science and Technology Program of Xiamen (3502Z20182005), Chinese Academy of Sciences-The World Academy of Sciences (CAS-TWAS) president's fellowship program for developing countries, and Youth Innovation Promotion Association CAS (2016280).

Appendix A. Supplementary data

Supplementary data related to this article can be found at <https://doi.org/10.1016/j.watres.2020.115857>.

References

- Abdolmaleki, A., Mallakpour, S., Borandeh, S., 2015. Efficient heavy metal ion removal by triazinyl- β -cyclodextrin functionalized iron nanoparticles. *RSC Adv.* 5, 90602–90608. <https://doi.org/10.1039/c5ra15134a>.
- Alsaiee, A., Smith, B.J., Xiao, L., Ling, Y., Helbling, D.E., Dichtel, W.R., 2016. Rapid removal of organic micropollutants from water by a porous beta-cyclodextrin polymer. *Nature* 529, 190–194. <https://doi.org/10.1038/nature16185>.
- Alzate-sanchez, D., Ling, Y., Li, C., Frank, B., Bleher, R., Fairbrother, D.H., Helbling, D., Dichtel, W., 2019. β -Cyclodextrin polymers on microcrystalline cellulose as a granular media for organic micropollutant removal from water. *ACS Appl. Mater. Interfaces*. <https://doi.org/10.26434/chemrxiv.7471508.v1>.
- Anastopoulos, I., Bhatnagar, A., Lima, E.C., 2016. Adsorption of rare earth metals: a review of recent literature. *J. Mol. Liq.* 221, 954–962. <https://doi.org/10.1016/j.molliq.2016.06.076>.
- Badruddoza, A.Z., Shawon, Z.B., Tay, W.J., Hidajat, K., Uddin, M.S., 2013. Fe₃O₄/cyclodextrin polymer nanocomposites for selective heavy metals removal from industrial wastewater. *Carbohydr. Polym.* 91, 322–332. <https://doi.org/10.1016/j.carbpol.2012.08.030>.
- Callura, J.C., Perkins, K.M., Noack, C.W., Washburn, N.R., Dzombak, D.A., Karamalidis, A.K., 2018. Selective adsorption of rare earth elements onto functionalized silica particles. *Green Chem.* 20, 1515–1526. <https://doi.org/10.1039/c8gc00051d>.
- Faria, P.C.C., Órfão, J.J.M., Pereira, M.F.R., 2004. Adsorption of anionic and cationic dyes on activated carbons with different surface chemistries. *Water Res.* 38, 2043–2052. <https://doi.org/10.1016/j.watres.2004.01.034>.
- Freundlich, H., 1907. Über die Adsorption in Lösungen. *Z. Phys. Chem.* 57U, 385–470. <https://doi.org/10.1515/zpch-1907-5723>.
- Gok, C., 2014. Neodymium and samarium recovery by magnetic nano-hydroxyapatite. *J. Radioanal. Nucl. Chem.* 301, 641–651. <https://doi.org/10.1007/s10967-014-3193-z>.
- Guo, Z., Li, Y., Pan, S., Xu, J., 2015. Fabrication of Fe₃O₄@cyclodextrin magnetic composite for the high-efficient removal of Eu (III). *J. Mol. Liq.* 206, 272–277. <https://doi.org/10.1016/j.molliq.2015.02.034>.
- Gwenzi, W., Mangori, L., Danha, C., Chaukura, N., Dunjana, N., Sanganyado, E., 2018. Sources, behaviour, and environmental and human health risks of high-technology rare earth elements as emerging contaminants. *Sci. Total Environ.* 636, 299–313. <https://doi.org/10.1016/j.scitotenv.2018.04.235>.
- Hasegawa, Y., Tamaki, S., Yajima, H., Hashimoto, B., Yaita, T., 2011. Selective separation of samarium(III) by synergistic extraction with β -diketone and methylphenylphenanthroline carboxamide. *Talanta* 85, 1543–1548. <https://doi.org/10.1016/j.talanta.2011.06.041>.
- Herrmann, H., Nolde, J., Berger, S., Heise, S., 2016. Aquatic ecotoxicity of lanthanum – a review and an attempt to derive water and sediment quality criteria. *Ecotoxicol. Environ. Saf.* 124, 213–238. <https://doi.org/10.1016/j.ecoenv.2015.09.033>.
- Ho, Y.S., McKay, G., 1999. Pseudo-second order model for sorption processes. *Process Biochem.* 34, 451–465. [https://doi.org/10.1016/S0032-9592\(98\)00112-5](https://doi.org/10.1016/S0032-9592(98)00112-5).
- Hu, X., Hu, Y., Xu, G., Li, M., Zhu, Y., Jiang, L., Tu, Y., Zhu, X., Xie, X., Li, A., 2020. Green synthesis of a magnetic β -cyclodextrin polymer for rapid removal of organic micro-pollutants and heavy metals from dyeing wastewater. *Environ. Res.* 180, 108796. <https://doi.org/10.1016/j.envres.2019.108796>.
- Jha, M.K., Kumari, A., Panda, R., Rajesh Kumar, J., Yoo, K., Lee, J.Y., 2016. Review on hydrometallurgical recovery of rare earth metals. *Hydrometallurgy* 161. <https://doi.org/10.1016/j.hydromet.2016.01.003>.
- Klemes, M.J., Ling, Y., Chiapasco, M., Alsaiee, A., Helbling, D.E., Dichtel, W.R., 2018. Phenolation of cyclodextrin polymers controls their lead and organic micro-pollutant adsorption. *Chem. Sci.* <https://doi.org/10.1039/c8sc03267j>.
- Lagergren, S., 1898. About the theory of so-called adsorption of soluble substances. *K. - Sven. Vetenskapsakademiens Handl.* 24, 1–39.
- Langmuir, I., 1918. The adsorption of gases on plane surfaces of glass, mica and platinum. *J. Am. Chem. Soc.* 40, 1361–1403. <https://doi.org/10.1021/ja02242a004>.
- Li, B., Jia, D., Zhou, Y., Hu, Q., Cai, W., 2006. In situ hybridization to chitosan/magnetite nanocomposite induced by the magnetic field. *J. Magn. Magn. Mater.* 306, 223–227. <https://doi.org/10.1016/j.jmmm.2006.01.250>.
- Li, L., Duan, Z., Chen, J., Zhou, Y., Zhu, L., Xiang, Y., Xia, D., 2017. Molecular recognition with cyclodextrin polymer: a novel method for removing sulfides efficiently. *RSC Adv.* 7, 38902–38910. <https://doi.org/10.1039/c7ra06782h>.
- Morin-Crini, N., Crini, G., 2013. Environmental applications of water-insoluble β -cyclodextrin-epichlorohydrin polymers. *Prog. Polym. Sci.* 38, 344–368. <https://doi.org/10.1016/j.progpolymsci.2012.06.005>.
- Nkinahamira, F., Su, T., Xie, Y., Ma, G., Wang, H., Li, J., 2017. High pressure adsorption of CO₂ on MCM-41 grafted with quaternary ammonium ionic liquids. *Chem. Eng. J.* <https://doi.org/10.1016/j.cej.2017.05.173>.
- Nkinahamira, F., Suanon, F., Chi, Q., Li, Y., Feng, M., Huang, X., Yu, C.-P., Sun, Q., 2019. Occurrence, geochemical fractionation, and environmental risk assessment of major and trace elements in sewage sludge. *J. Environ. Manag.* 249, 109427. <https://doi.org/10.1016/j.jenvman.2019.109427>.
- Pagano, G., Guida, M., Siciliano, A., Oral, R., Koçbaş, F., Palumbo, A., Castellano, I., Migliaccio, O., Thomas, P.J., Trifuoggi, M., 2016. Comparative toxicities of selected rare earth elements: sea urchin embryogenesis and fertilization damage with redox and cytogenetic effects. *Environ. Res.* 147, 453–460. <https://doi.org/10.1016/j.envres.2016.02.031>.
- Pearson, R.G., 1968. Hard and soft acids and bases, HSAB, part 1: fundamental principles. *J. Chem. Educ.* 45. <https://doi.org/10.1021/ed045p581>.
- Qi, X.H., Du, K.Z., Feng, M.L., Gao, Y.J., Huang, X.Y., Kanatzidis, M.G., 2017. Layered A₂Sn₃S₇·1.25H₂O (A = organic cation) as efficient ion-exchanger for rare earth element recovery. *J. Am. Chem. Soc.* 139, 4314–4317. <https://doi.org/10.1021/jacs.7b00565>.
- Qiu, S., Zhao, S., Sun, X., 2016. Development of magnetic silica hybrid material with P507 for rare earth adsorption. *J. Chem. Eng. Data* 62, 469–476. <https://doi.org/10.1021/acs.jced.6b00764>.
- Reddy, D.H.K., Lee, S.M., 2013. Application of magnetic chitosan composites for the removal of toxic metal and dyes from aqueous solutions. *Adv. Colloid Interface Sci.* 201–202, 68–93. <https://doi.org/10.1016/j.cis.2013.10.002>.
- Saha, P., Chowdhury, S., 2011. Insight into adsorption thermodynamics. In: *Thermodynamics*. InTech. <https://doi.org/10.5772/13474>.
- Su, C., 2017. Environmental implications and applications of engineered nanoscale magnetite and its hybrid nanocomposites: a review of recent literature. *J. Hazard Mater.* 322, 48–84. <https://doi.org/10.1016/j.jhazmat.2016.06.060>.
- Tran, H.N., You, S.-J., Chao, H.-P., 2016. Thermodynamic parameters of cadmium adsorption onto orange peel calculated from various methods: a comparison study. *J. Environ. Chem. Eng.* 4, 2671–2682. <https://doi.org/10.1016/j.jece.2016.05.009>.
- Tran, H.N., You, S.J., Hosseini-Bandegharaei, A., Chao, H.P., 2017. Mistakes and inconsistencies regarding adsorption of contaminants from aqueous solutions: a critical review. *Water Res.* 120, 88–116. <https://doi.org/10.1016/j.watres.2017.04.014>.
- Tsiepe, J.T., Mamba, B.B., Inamuddin, Abd-El-Aziz, A.S., Mishra, A.K., 2018. Fe₃O₄– β -

- cyclodextrin–chitosan bionanocomposite for arsenic removal from aqueous solution. *J. Inorg. Organomet. Polym. Mater.* 28, 467–480. <https://doi.org/10.1007/s10904-017-0741-3>.
- U.S. department of energy, 2011. *Critical Materials Strategy Report* ([WWW Document]).
- U.S. Geological Survey, 2019. *Rare Earths Statistics and Information* ([WWW Document]).
- Wang, Q., Wilfong, W.C., Kail, B.W., Yu, Y., Gray, M.L., 2017. Novel poly-ethylenimine–acrylamide/SiO₂ hybrid hydrogel sorbent for rare-earth-element recycling from aqueous sources. *ACS Sustain. Chem. Eng.* 5, 10947–10958. <https://doi.org/10.1021/acssuschemeng.7b02851>.
- Weber, T.W., Chakravorti, R.K., 1974. Pore and solid diffusion models for fixed-bed adsorbers. *AIChE J.* 20, 228–238. <https://doi.org/10.1002/aic.690200204>.
- Yirsaw, B.D., Megharaj, M., Chen, Z., Naidu, R., 2016. Environmental application and ecological significance of nano-zero valent iron. *J. Environ. Sci.* 44, 88–98. <https://doi.org/10.1016/j.jes.2015.07.016>.
- Zhang, H., McDowell, R.G., Martin, L.R., Qiang, Y., 2016. Selective extraction of heavy and light lanthanides from aqueous solution by advanced magnetic nanosorbents. *ACS Appl. Mater. Interfaces* 8, 9523–9531. <https://doi.org/10.1021/acsami.6b01550>.
- Zhang, W., Lin, M., Wang, M., Tong, P., Lu, Q., Zhang, L., 2017. Magnetic porous beta-cyclodextrin polymer for magnetic solid-phase extraction of microcystins from environmental water samples. *J. Chromatogr. A*. <https://doi.org/10.1016/j.chroma.2017.04.063>.
- Zheng, X., Wang, C., Dai, J., Shi, W., Yan, Y., 2015. Design of mesoporous silica hybrid materials as sorbents for the selective recovery of rare earth metals. *J. Mater. Chem.* 3, 10327–10335. <https://doi.org/10.1039/c4ta06860b>.
- Zhu, B., Wu, D., Yang, Y., Chen, Y., Li, W., Guo, J., Wang, Q., 2011. Selective removal of La(III) ions using super-paramagnetic nanosorbent coated by saponified sec-octylphenoxy acetic acid. *J. Chem. Eng. Data* 57, 553–560. <https://doi.org/10.1021/je201122f>.